Int. J. Electrochem. Sci., 15**(2020)** 9313 – 9324, doi: 10.20964/2020.09.70

International Journal of ELECTROCHEMICAL SCIENCE
www.electrochemsci.org

Electrochemical Dissolution Behavior of Ti-48Al-2Nb-2Cr in $NaNO_3$ and NaCl Electrolytes

Hao Wang[#], *Jia Liu*[*#], *Dawei Gu, Di Zhu*

College of Mechanical and Electrical Engineering, Nanjing University of Aeronautics and Astronautics, Nanjing, 210016, China
[*]E-mail: meejliu@nuaa.edu.cn
#These authors contribute equally.

Received: 2 March 2020 / *Accepted:* 6 July 2020 / *Published:* 10 August 2020

Ti-48Al-2Nb-2Cr (TiAl4822) intermetallic material is an excellent lightweight and high-temperature alloy used in the aerospace industry. Electrochemical machining (ECM) is one of the most significant processing technologies for the manufacturing of TiAl intermetallics. A comprehensive understanding of the electrochemical dissolution behavior of TiAl4822 alloys is critical for the optimization of electrolyte composition and processing parameters. This study investigates the electrochemical dissolution behavior of TiAl4822 to improve machining efficiency and surface quality obtained by ECM. Polarization and current efficiency curves of TiAl4822 in $NaNO_3$ and NaCl electrolytes at different temperatures and concentrations were analyzed. To compare electrochemical dissolution behavior in two electrolytes, we performed single-factor experiments by varying one of the following parameters in a single experiment: applied voltage, duty ratio, frequency, electrode feed rate, and electrolyte temperature. The experimental results show that TiAl4822 has a higher material removal rate in NaCl and a higher surface quality in $NaNO_3$.

Keywords: Ti-48Al-2Nb-2Cr, Electrochemical machining, Electrochemical dissolution behavior, polarization curve, single-factor experiment

1. INTRODUCTION

Excellent physical properties, such as low density and resistance to oxidation and corrosion at high temperatures, favor the application of the TiAl4822 intermetallic alloy in high-demanding areas like in aerospace industry [1, 2]. However, high hardness at room temperature makes TiAl4822 extremely difficult to cut and shape for specific purpose by traditional machining [3, 4]. Based on a controlled electrochemical anodic reaction, non-traditional ECM technology offers high efficiency and surface integrity, and the absence of tool wear, regardless of the material hardness and ductility [5- 7]. ECM is also cost-effective in comparison with traditional cutting technology, such as turning, grinding,

and high-speed milling [8, 9]. General Electric (GE) chose the ECM as a precision machining technology to process TiAl4822 turbine blades in GEnx aero engines [10], and the ECM became the central processing technology for TiAl4822 intermetallics.

The improvement of the machining quality of TiAl intermetallics in the ECM technology was extensively studied. Memarbashi investigated the passivation behavior of γ-TiAl in different oxidizing and non-oxidizing acidic solutions [11]. Klocke studied the influence of current density on DC electrochemical machinability of γ-TiAl-based alloys [12], and compared electrochemical machinability of electron beam-melted and cast gamma titanium aluminide TNB-V5 [13]. Liu assessed the effect of ECM process parameters of γ-TiAl by orthogonal experiments [14]. Clifton determined optimal and reproducible ECM parameters of γ-TiAl in perchlorate and chloride electrolytes [15]. Souza studied the effect of Ti amount on electrochemical behavior [16], while He evaluated the machining accuracy of γ-TiAl alloys in pulsed wire ECM [17]. Delgado-Alvarado discussed the corrosion behavior of TiAl4822 in Ringer's solution and found that corrosion resistance of TiAl4822 can be improved by surface oxidation at 500 °C [18]. Finally, Wang assessed the electrochemical dissolution behavior of a TiAl 45XD alloy in NaCl and $NaNO_3$ solutions and proposed qualitative models to describe the electrochemical dissolution behavior [19]. Wang also studied the difference of dissolution behaviors of extruded and cast Ti-48Al-2Cr-2Nb alloys in $NaNO_3$ solution [20].

Previous research focused on machinability and optimization of the ECM parameters of TiAl intermetallics. However, a systematic study of TiAl4822 electrochemical dissolution characteristics during the ECM process is rather scarce. Understanding the electrochemical dissolution behavior of TiAl4822 alloys is critical for the selection of the appropriate electrolyte composition and processing parameters. To comprehend the characteristics of the TiAl4822 ECM process, the electrochemical dissolution behavior of the TiAl4822 alloy in $NaNO_3$ and NaCl electrolytes was investigated. The polarization and current efficiency curves measurements, as well as single-factor experiments with parameters of applied voltage, duty ratio, frequency, electrode feed rate, and electrolyte temperature were performed.

2. EXPERIMENTAL

2.1. Material

To avoid compositional fluctuations that might affect the results of the test, we used the same TiAl4822 rod to prepare all specimens. The composition of the TiAl4822 alloy is given in Table 1.

Table 1. The composition of the TiAl4822 alloy.

Element	Ti	Al	Nb	Cr
Percent/wt.%	65.5	26.3	4.3	3.9

2.2. Polarization studies

The determination of polarization behavior is commonly used to study electrochemical dissolution; herein, the polarization behavior was tested in an electrochemical workstation CHI660D, and every sample was cut in a 10 mm × 10 mm × 10 mm cube, and the exposed surface was polished to a mirror finish.

The experiment was performed in a three-electrode glass cell; a standard calomel electrode (SCE), and a standard platinum sheet were used as reference and counter electrode, respectively [21]. The anodic polarization curves were recorded with a potential scanning rate of 10mV/s [22].

2.3. Current efficiency

Current efficiency is an essential characteristic of dissolution behavior. It indicates a volume of removed material at a different current density per unit time and unit area [23]. Accurate measurement of the current efficiency has a great significance for the analysis of material dissolution, machining accuracy improvement, and optimal cathode design [24, 25]. To study the dissolution efficiency of TiAl4822, we measured the current efficiency of TiAl4822 in $NaNO_3$ and NaCl electrolytes. The measurement device is shown in Fig. 1. The cathode is a metal block with a flat end, and the anode workpiece is a rectangular bar with a 16 mm × 16 mm section. During the measurement, the cathode remains fixed while the workpiece is continuously fed to the cathode at a constant speed. A constant voltage is applied between the electrodes, and the electrolyte is pumped into the inter-electrode gap. Over time, the dissolution rate of the workpiece and the cathode feeding rate reach equilibrium. In this state, the current does not change anymore.

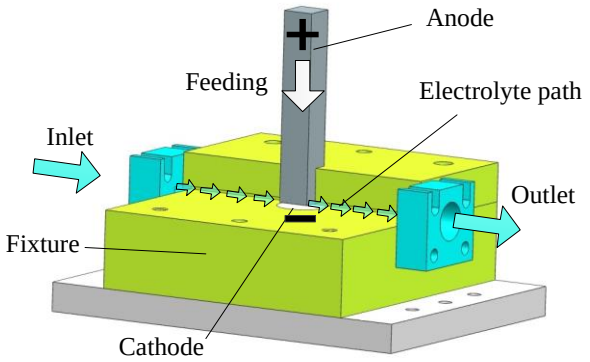

Figure 1. The device for the measurement of current efficiency curves.

By measuring stable current density, i, at different feeding rates, current efficiency, η, can be obtained by the equation below [26]:

$$v_a = \eta\omega i \quad (1)$$

$$\eta\omega = \frac{v_a}{i} \quad (2)$$

where ω is the theoretical value of the volume electrochemical equivalent, and v_a is the corrosion rate of the workpiece, which is equal to the feeding rate of the cathode in the equilibrium state. Since a direct measurement of ω is not straightforward, the parameter $\eta\omega$ is used to describe

current efficiency. By measuring current at different feeding rates, the complete current efficiency curve can be obtained.

2.4. Single-factor experiments

To better understand the ECM process of TiAl4822, single-factor experiments were performed using the experimental facility showed in Fig. 2 and the selected workpiece. The fixture was made of epoxy resin, while the cathode was of stainless steel. The specimens were TiAl4822 blocks with a cross-section of 15 mm × 10 mm. The workpiece was fixed in the fixture while the cathode tool was fed toward the workpiece. From the inlet, the electrolyte flows through the inter-electrode gap and releases the experimental facility through the outlet on the other side. The cathode was connected to the negative pole and the workpiece to the positive pole of the power supply. Under the electrochemical reaction, the electrolyte gradually dissolves the workpiece with the continuous feeding of the cathode.

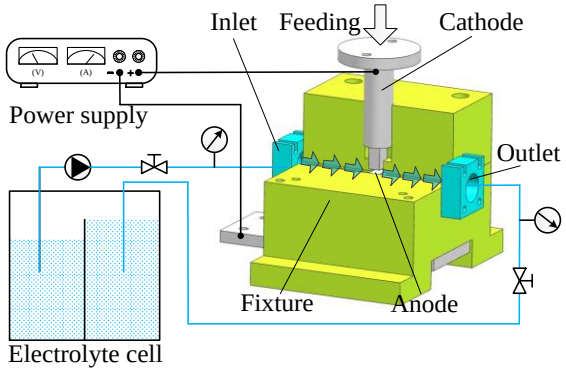

Figure 2. The experimental facility for the single-factor experiments.

The single-factor experiments were performed in 10 wt.% NaCl and 20 wt.% $NaNO_3$ by varying several parameters: applied voltage, electrode feed rate, electrolyte temperature, duty ratio, and frequency. During the single-factor experiments, starting values of voltage, electrode feed rate, frequency, electrolyte temperature, duty ratio, inlet pressure, and outlet pressure were set as 30 V, 1 mm/min, 1 kHz, 30°C, 50%, 0.8 MPa, and 0.1 MPa, respectively. The levels and values of the parameters studied in the single-factor experiments are listed in Table 2.

Table 2. The experimental parameters and levels.

Symbol	Parameter	Level			
		1	2	3	4
1	Applied voltage (V)	20	25	30	35
2	Electrode feed rate (mm/min)	0.5	1.0	1.5	2.0
3	Electrolyte temperature (°C)	20	25	30	35
4	Duty ratio (%)	25	50	75	100
5	Frequency (kHz)	0.25	0.50	0.75	1.00

3. RESULTS AND DISCUSSION

3.1. Polarization curves

The anodic polarization curves of TiAl4822 were measured in NaCl and $NaNO_3$ at different temperatures and concentrations, Figs. 3 and 4, respectively. It can be seen that the polarization curves in both electrolytes reach the self-corrosion potential of the anode and subsequently enter a stable passivation region with an increase of the potential. Afterward, the voltage reaches the potential of pitting corrosion, E_{pit}, when the passivation film breaks and pitting appears [27-29]. Finally, the current increases linearly with the voltage, and the anode material continuously dissolves in the electrolyte.

As Figs. 3 and 4 show, the value of E_{pit} is about 0.5 V in NaCl and 2 V in $NaNO_3$, indicating that the corrosion resistivity of TiAl4822 in $NaNO_3$ is higher than in NaCl. This implies that chloride ions are more aggressive toward the passivation film than nitrate ions. As the temperature increases from 20 to 40°C, E_{pit} decreases about 0.2 V in both electrolytes, which is connected with the rise of chemical activity at elevated temperatures. The results also show that the concentration of electrolyte has no significant effect on the E_{pit} value of TiAl4822.

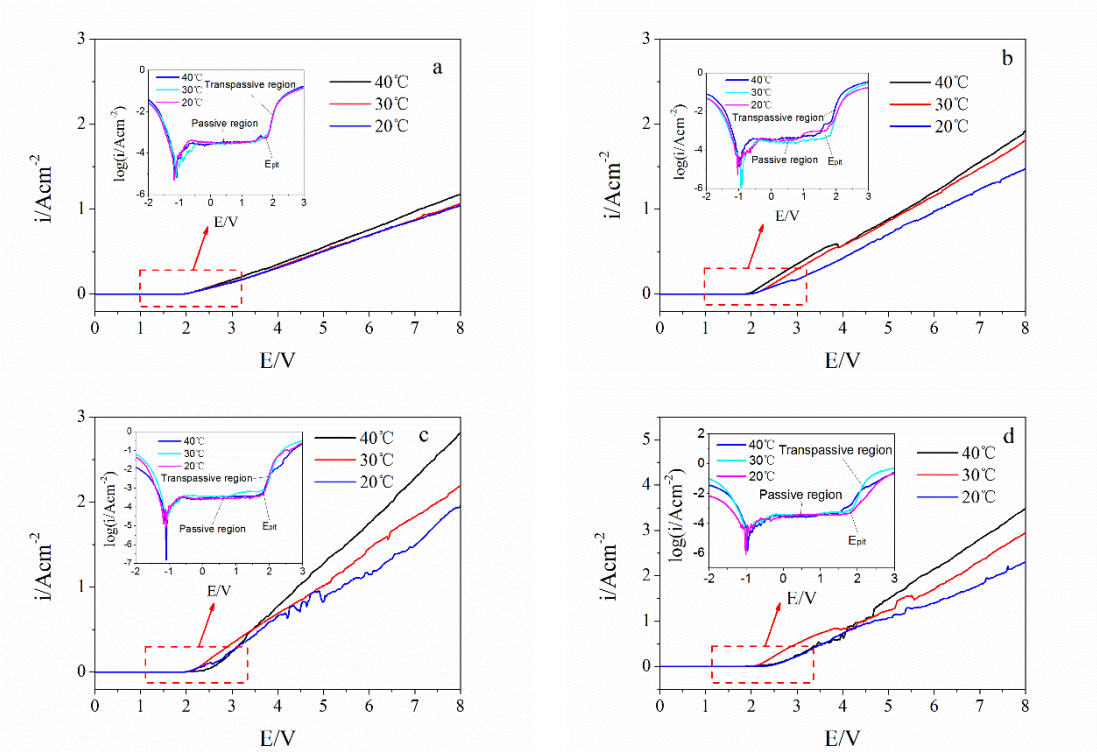

Figure 3. The polarization curves of TiAl4822 in (a) 5wt.%, (b) 10wt.%, (c) 15wt.%, and (d) 20wt.% $NaNO_3$.

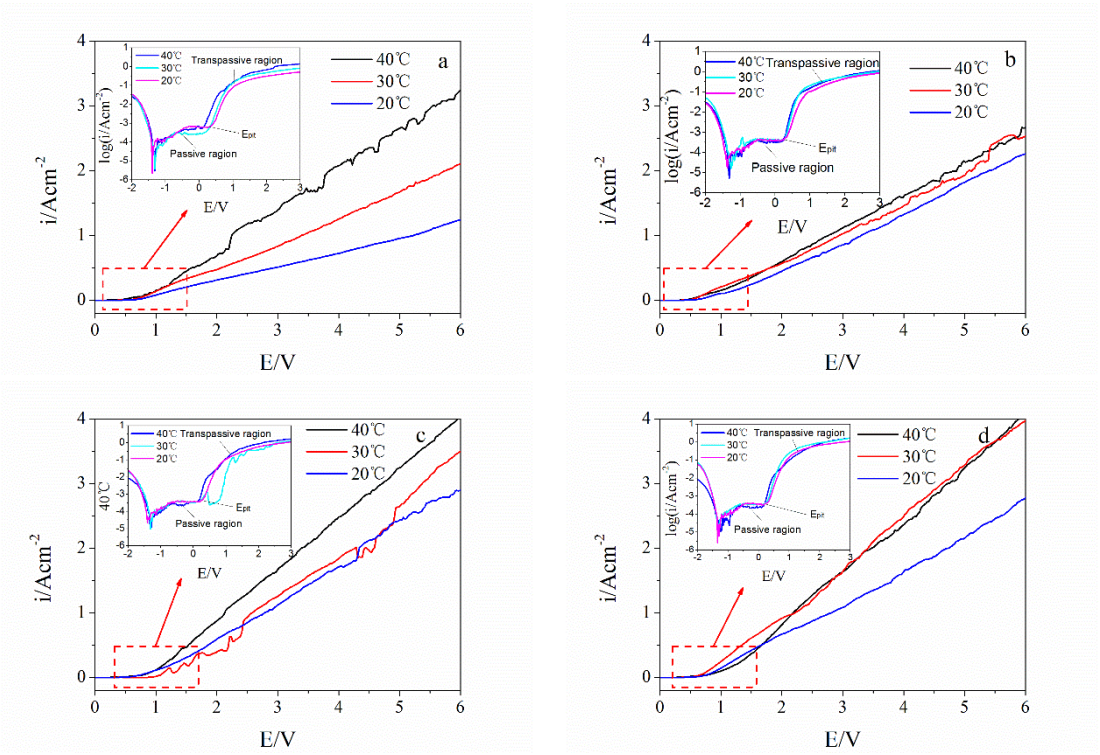

Figure 4. The polarization curves of TiAl4822 in (a) 5wt.%, (b) 10wt.%, (c) 15wt.%, and (d) 20wt.% NaCl.

3.2. The current efficiency measurements

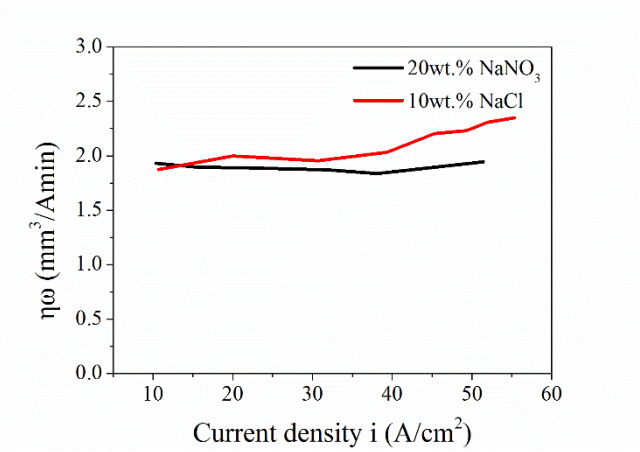

Figure 5. *ηω-i* curves of TiAl4822 in different electrolytes.

The *ηω-i* curves of TiAl4822 in NaCl and $NaNO_3$ electrolytes are shown in Fig. 5. In NaCl, the value of *ηω* slightly increases with the current density, while it is almost constant in $NaNO_3$. A possible explanation for this difference might be that valence of the element has decreased at high current density in NaCl [20]. The average value of current efficiency in NaCl is higher than that in $NaNO_3$, which reflects a more substantial corrosive effect of chloride than nitrate ions, and it is consistent with conclusion reported by Haisch [30]. The current efficiency curves indicate that ECM of

TiAl4822 in the NaCl solution has a higher processing efficiency than in $NaNO_3$ at the same processing conditions.

3.3. Single-factor experiments

Electrolyte conductivity is an important parameter that affects dissolution behavior [31]. Fig. 6 shows the evolution of conductivity with temperature of NaCl and $NaNO_3$ electrolytes at different concentrations. The conductivity of both electrolytes increases linearly with temperature. Higher concentration yields higher conductivity and lower ohmic resistance of both electrolytes. The concentration effect on conductivity was more significant for the NaCl than for the $NaNO_3$ electrolyte. This can be related to the small relative molecular mass of NaCl. To compare the electrochemical dissolution behaviors of TiAl4822 in NaCl and $NaNO_3$, 10 wt.% NaCl and 20 wt.% $NaNO_3$ solutions were selected since they have similar conductivity.

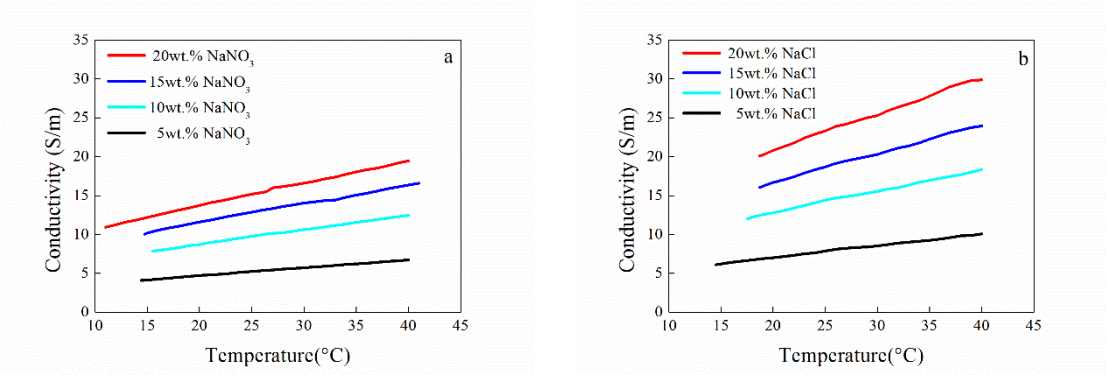

Figure 6. The conductivity of (a) $NaNO_3$ and (b) NaCl at different concentrations.

The single-factor experiments were successfully performed without short-circuiting. To study the dissolution characteristics of TiAl4822 in two electrolytes, the surface roughness (SR) of the workpiece and the machining gap (MG) in the equilibrium state were investigated. The size of MG was obtained by tool set, and the value of SR was obtained by measuring with a Perthometer M1 (Mahr) roughmeter.

In ECM, the selection of correct electrical parameters may help to improve the machining quality and obtain suitable MG [32]. Fig. 7 shows the relationship between MG and electrical parameters. It can be seen that MG increases with the processing voltage and duty ratio at constant values of other parameters. The voltage increase from 20 to 35 V induces the increase of the MG value from 0.24 to 0.502 mm in $NaNO_3$ and from 0.102 to 0.358 mm in NaCl. The change of the duty ratio from 25 to 100% increases the MG from 0.084 to 0.619 mm in $NaNO_3$ and from 0.11 to 0.657 mm in NaCl. However, the effect of frequency on MG is negligible. This can be understood in the sense of the average voltage, which is affected by both the applied voltage and the duty ratio but not by the frequency.

The electrical parameters also affect the surface quality of the workpiece. Fig. 8 shows the influence of electrical parameters on SR in NaCl and $NaNO_3$. The rise of the applied voltage from 20

to 35 V slightly improves the surface quality of TiAl4822 in both electrolytes, where SR decreases by 0.058 μm in $NaNO_3$ and 0.094 μm in NaCl. SR of TiAl4822 exhibits an opposite trend in two electrolytes with the frequency: the surface quality of the workpiece improves in $NaNO_3$ while it descends in NaCl as the frequency rises. A lower duty ratio, Fig. 8(c), enhances the surface quality of TiAl4822 at voltage and frequency of 30 V and 1000 Hz, respectively. However, SR increases rapidly from 0.301 to 0.703 μm if the duty ratio reduces from 50 to 25%. The effect may be caused by the change of MG, which decreases from 0.376 to 0.084 mm for the same variation of the duty ratio, being inappropriate for the removal of electrolytic products, which yields a poor surface quality in ECM [33].

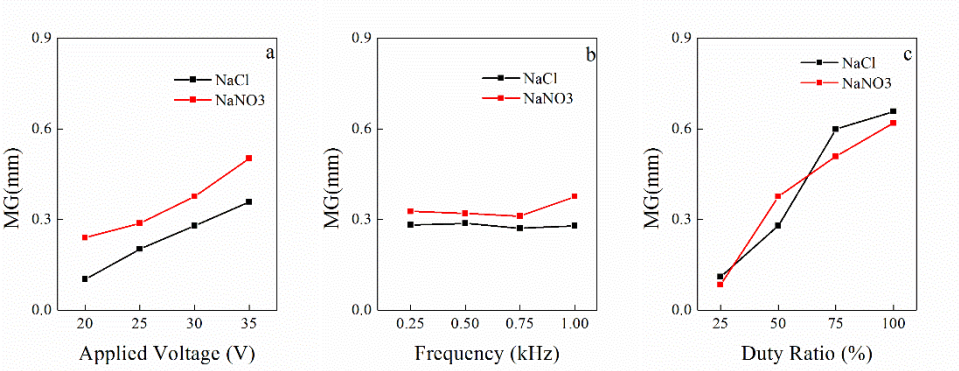

Figure 7. The influence of electrical parameters on MG in NaCl and $NaNO_3$.

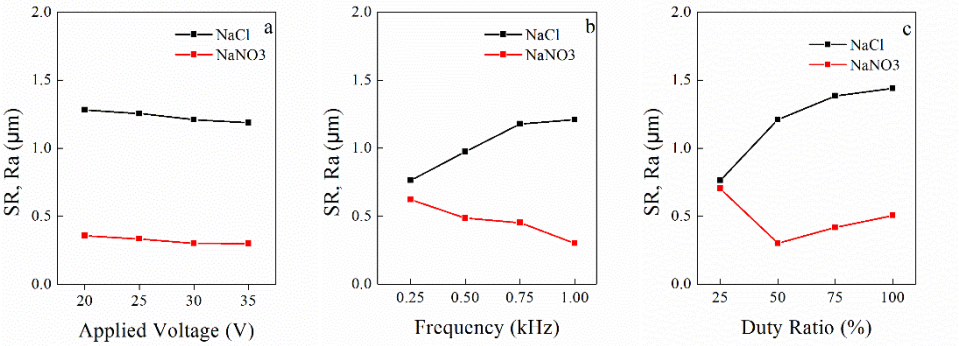

Figure 8. The influence of electrical parameters on SR in NaCl and $NaNO_3$.

The influence of the electrode feed rate and electrolyte temperature on MG and SR of TiAl4822 is also evaluated. With the increase of the electrode feed rate from 0.5 to 2 mm/min, MG decreases from 0.837 to 0.088 mm in $NaNO_3$ and from 0.625 to 0.087 mm in NaCl, being inversely proportional in both cases, Fig. 9(a). The temperature does not significantly influence MG, Fig. 9(b), and the value of MG maintained at about 0.3 mm in both electrolytes.

The changes of SR with the electrode feed rate and electrolyte temperature in NaCl and $NaNO_3$ electrolytes are shown in Fig. 10. As Fig. 10(a) shows, SR reduces with the electrode feed rate in NaCl since the higher electrode feed rate yields smaller MG, and thus, higher machining current and better surface quality [34]. When the electrode feed rate reaches 2 mm/min, SR decreases to 0.713 μm. In $NaNO_3$, SR decreases by 0.028 μm if the electrode feed rate increases from 0.5 to 1.0 mm/min.

However, as the feed rate increases from 1.0 to 1.5 mm/min, SR rapidly increases from 0.301 to 0.610 μm and then continuously grows further. The reason for this may be a higher density of $NaNO_3$ solution and its poor flow performance in the case of small MG. Above 1.5 mm/min, MG is less than 0.164mm and SR is over 0.5 μm. In both electrolytes, the surface quality of TiAl4822 can be improved by increasing electrolyte temperature, and the effect is stronger in NaCl than in $NaNO_3$, Fig. 10(b).

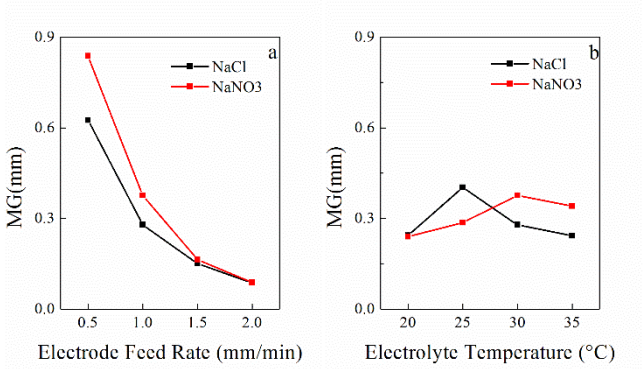

Figure 9. The influence of the electrode feed rate and electrolyte temperature on MG in NaCl and $NaNO_3$.

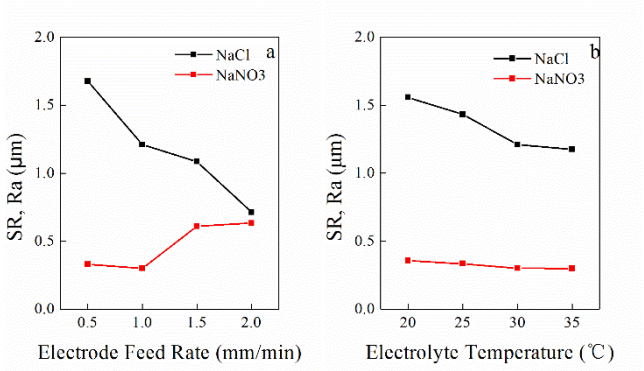

Figure 10. The influence of the electrode feed rate and electrolyte temperature on SR in NaCl and $NaNO_3$.

Conclusively, TiAl4822 exhibits higher surface quality in $NaNO_3$ than in NaCl under the same processing conditions. For achieving a higher surface quality of TiAl4822, the selected machining parameters should ensure that MG is not lower than 0.3 mm.

Cross-sections of specimens obtained at different electrode feed rates are shown in Figs. 11 and. 12. It can be observed that no inter-crystalline corrosion occurs during the ECM process in both NaCl and $NaNO_3$ electrolytes.

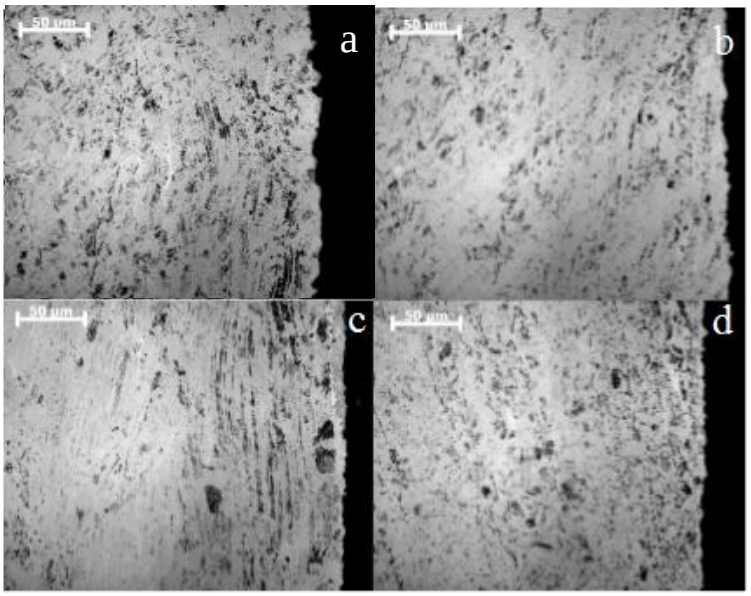

Figure 11. The cross-sectional analysis of TiAl4822 in NaCl at different electrode feed rates (a. 0.5, b. 1.0, c. 1.5, and d. 2.0 mm/min).

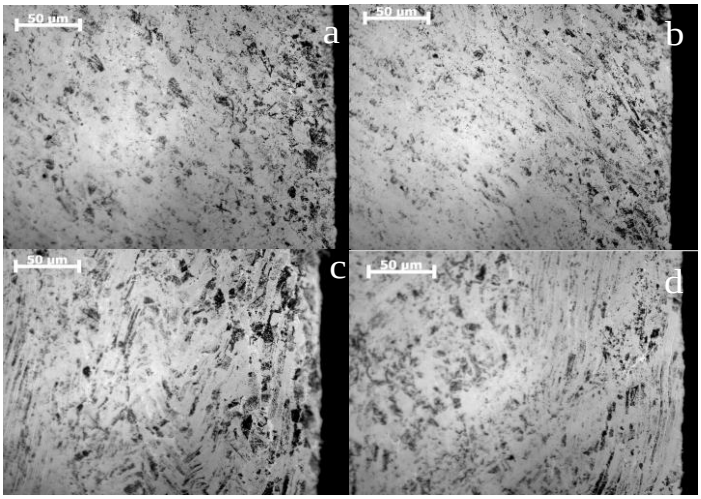

Figure 12. The cross-sectional analysis of the TiAl4822 in $NaNO_3$ at different electrode feed rates (a. 0.5, b. 1.0, c. 1.5, and d. 2.0 mm/min).

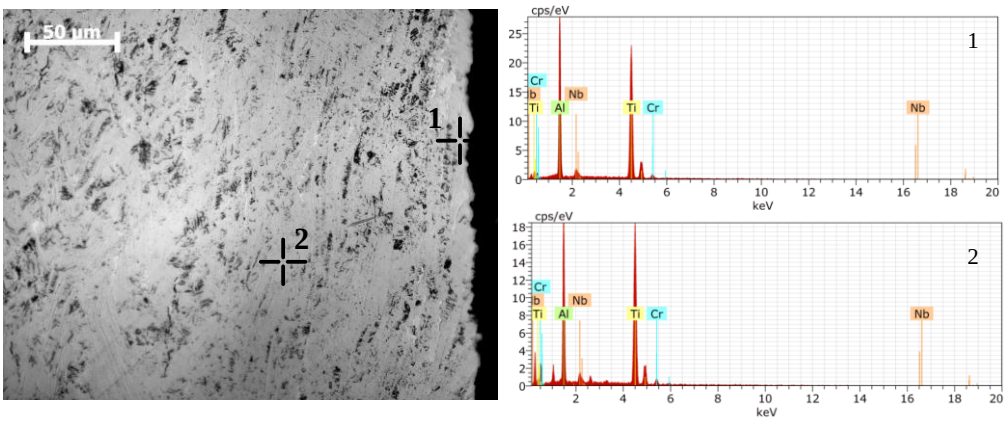

Figure 13. The EDX analysis of the TiAl4822 cross-section in NaCl.

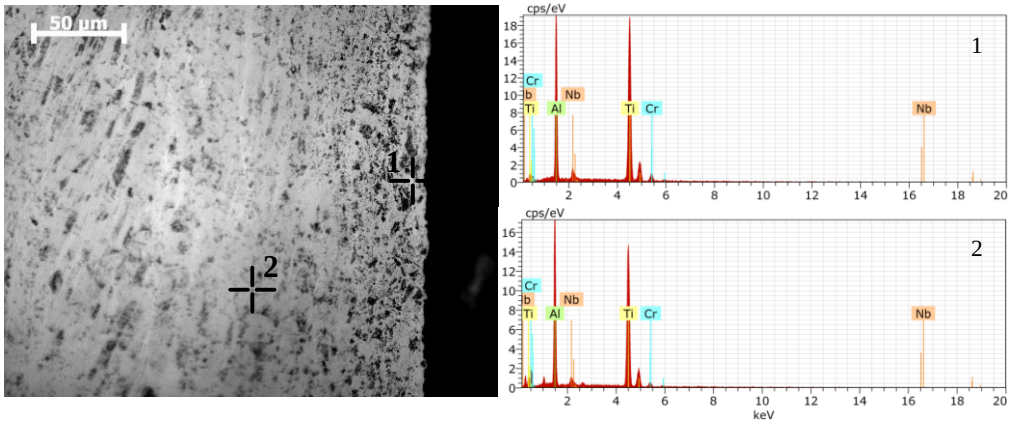

Figure 14. The EDX analysis of the TiAl4822 cross-section in $NaNO_3$.

Furthermore, the EDX analysis was used to investigate whether elements of the TiAl4822 rim zone are affected by electrolytes during ECM. As shown in Figs. 13 and 14, the points in the central part of the workpiece and near the processing area were selected. The results indicate that the elemental composition of the TiAl4822 rim zone is consistent with that of the matrix, which implies that the anodic oxidation reaction does not form a tightly bound film on the surface of TiAl4822 after ECM process.

4. CONCLUSIONS

In this study, the electrochemical dissolution behavior of TiAl4822 in different electrolytes was investigated. The results can be summarized as follows:

1. The polarization curves show that the temperature rise decreases corrosion resistance in both $NaNO_3$ and NaCl electrolytes. Besides, TiAl4822 has a higher E_{pit} values in $NaNO_3$ than in NaCl at the same temperature.

2. In both NaCl and $NaNO_3$ electrolytes, current efficiency changes little with current density. The higher current efficiency in NaCl than in $NaNO_3$ at the same conditions indicates the faster material removal rate in NaCl.

3. The single-factor experiments were conducted both in NaCl and $NaNO_3$, and the influence of various parameters on SR and MG of the TiAl4822 ECM process was analyzed. The results show that the higher surface quality is obtained in $NaNO_3$ than in NaCl under the same conditions. The decrease of the applied voltage, duty ratio, and the increase of the electrode feed rate, small MG can be obtained. However, MG should be kept at least as high as 0.3 mm; otherwise, too small MG will yield an impaired removal of electrolytic products and reduce the surface quality of the workpiece.

4. The EDX analysis proved that ECM does not affect the material composition of the TiAl4822 rim zone and that inter-granular corrosion does not occur.

ACKNOWLEDGMENTS
This work was supported by the Fundamental Research Funds for the Central Universities (NS2019032).

References

1. B.P. Bewlay, S. Nag, A. Suzuki and M. J. Weimer,*Mater. High Temp.*, 33 (2016) 549.
2. M. Seifi, A.A. Salem , D.P. Satko , U.Ackelid , S.L. Semiatin and J.J. Lewandowski, *J. Alloy. Compd.*, 729 (2017) 1118.
3. A.L. Mantle, D.K. Aspinwall andJ. Mater,*Process. Technol.*, 118 (2001) 143.
4. D.K. Aspinwall, R.C. Dewes, A.L. Mantle, *CIRP Ann. Manuf. Technol.*, 54 (2005) 99.
5. F. Klocke, M. Zeis, A. Klink andD.Veselovac, *Procedia Cirp*, 6 (2013) 368.
6. K.P. Rajurkar, D. Zhu, J.A. Mcgeough, J.Kozak, A.De Silvad, *CIRP Ann. Manuf. Technol.*, 48 (1999) 567.
7. Z.Y. Xu, Y.D. Wang, *Chin. J. Aeronaut.*, (2019) doi: 10.1016/j.cja.2019.09.016.
8. F. Klocke, L. Settineri, D. Lung, P.C. Priarone and M. Arft, *Wear*, 302 (2013) 1136.
9. A. Schubert, U. Götze, M. Hackert-Oschätzchen, N. Lehnert, F. Herold, G. Meichsner and A. Schmidt, *IOP Conf. Series: Materials Science and Engineering*, 118 (2016), 012035
10. S. Trimble, *Flight International*, 183 (2013) 12.
11. S.Memarbashi, E. Saebnoori and T. Shahrabi,*J. Mater. Eng. Perform.*, 23 (2014) 912.
12. F. Klocke, T. Herrig, M. Zeis and A. Klink, *Procedia Cirp*, 35 (2015) 50.
13. F. Klocke, T. Herrig, M. Zeis and A. Klink, *Proc. Inst. Mech. Eng. Part B-J. Eng. Manuf.*, 232 (2018) 586.
14. J. Liu, D. Zhu, L. Zhao and Z.X. Yang, *Procedia Cirp*, 35 (2015) 20.
15. D. Clifton, A.R. Mount, D.J. Jardine and R. Roth, *J. Mater. Process. Technol.*, 108 (2001) 338.
16. K.A.D. Souza and A. Robin, *Mater. Chem. Phys.*, 103 (2007) 351.
17. H. He, N.S. Qu, Y.B. Zeng, X.L. Fang and Y.Y. Yao, *Int. J. Adv. Manuf. Technol.*, 86 (2016) 2353.
18. C. Delgado-Alvarado and P.A. Sundaram, *Acta Biomater.*, 2 (2006) 701.
19. Y.D. Wang, Z.Y. Xu and A. Zhang, *Corrosion Sci.*, 157 (2019) 357.
20. Y.D. Wang, Z.Y. Xu and A. Zhang, *J. Electrochem. Soc.*, 166 (2019) E347.
21. N. Peng, Y.Q. Wen and Y.D. He, *SN Applied Sciences*, 1 (2019) 88.
22. Y.F. He, W.Z. Lu, W.M. Gan, J.S. Zhao and D.W. Zuo, *Proc. Inst. Mech. Eng. Pt. L-J. Mater.-Design Appl.*, 232 (2018) 602.
23. D.T. Chin and A.J.J. Wallace, *J. Electrochem. Soc.*, 120 (1973) 1487.
24. T. Fujisawa,K. Inaba, M. Yamamoto andD. Kato,*J. Fluids Eng.*, 130 (2008) 081602.
25. L.G. Yu, D. Zhu, Y.J. Yang and J.B. Zhao, *Proc. Inst. Mech. Eng. Part B-J. Eng. Manuf.*, 234 (2019) 814.
26. L. Tang, B. Li, S. Yang, Q.L. Duan and B.Y. Kang, *Int. J. Adv. Manuf. Technol.*, 71 (2014) 1825.
27. D.Y. Wang, Z.W. Zhu, N.F. Wang, D. Zhu and H.R. Wang, *Electrochim. Acta*, 156 (2015) 301.
28. H. Luo, H.Z. Su, B.S. Li and G.B. Ying, *Appl. Surf. Sci.*, 439 (2018) 232.
29. W.D. Liu, S.S. Ao, Y. Lia, Z.M. Liu, H. Zhang, S.M. Manladan, Z. Luo and Z.P. Wang, *Electrochim. Acta*, 233 (2017) 190.
30. T. Haisch, E. Mittemeijer and J.W. Schultze, *Electrochim. Acta*, 47 (2001) 235.
31. V.K. Jain, A.K. Chouksey, *Proc. Inst. Mech. Eng. Part B-J. Eng. Manuf.*, 232 (2018) 2449.
32. T.M.C. Jegan and D. Ravindran, *Comput. Intell.*, 33 (2017) 1019.
33. H. Wang, D. Zhu and J. Liu, *CIRP Ann-Manuf. Technol.*, 68 (2019) 165.
34. J.C.D.S. Neto, E.M.D. Silva and M.B.D. Silva, *J. Mater. Process. Technol.*, 179 (2006) 92.